



# Sono-assisted synthesis of nanostructured polyaniline for adsorption of aqueous Cr(VI): Effect of protonic acids



Jing Wang<sup>a,b,\*</sup>, Kaka Zhang<sup>c</sup>, Liang Zhao<sup>a,b</sup>

<sup>a</sup> Institute of Chemistry, Henan Academy of Sciences, Zhengzhou 450002, PR China

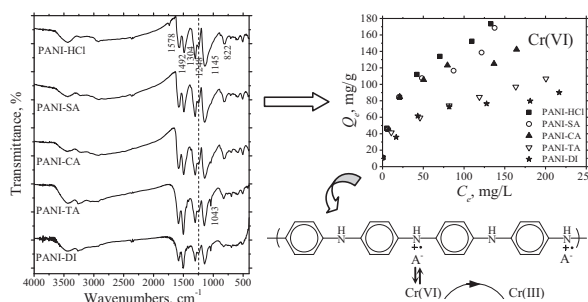
<sup>b</sup> High & New Technology Research Center, Henan Academy of Sciences, Zhengzhou 450002, PR China

<sup>c</sup> School of Material Science and Engineering, Zhengzhou University, Zhengzhou 450001, PR China

## HIGHLIGHTS

- Nanostructured PANIs were prepared by a facile sono-assisted method.
- Protonic acids impacted PANI morphology and molecular structure.
- PANIs varied in Cr(VI) adsorption properties depending on protonic acids.
- A mechanism of electrostatic adsorption followed by Cr(VI) reduction was proposed.

## GRAPHICAL ABSTRACT



## ARTICLE INFO

### Article history:

Received 15 August 2013

Received in revised form 31 October 2013

Accepted 4 November 2013

Available online 15 November 2013

### Keywords:

Nanostructured polyaniline

Molecular structure

Protonic acid

Cr(VI)

Adsorption

Reduction

## ABSTRACT

Polyaniline (PANI) nanoparticles and 1D nanostructures were prepared by a facile sono-assisted chemical oxidation method in protonic acids like HCl, surfulamic acid (SA), citric acid (CA), taurine (TA) and neutral deionized (DI) water for removal of aqueous Cr(VI). Results showed that all the prepared PANI nanostructures showed efficient adsorption for Cr(VI), however, their adsorption efficiencies varied depending on the protonic acids and the consequent molecular structures of PANIs. Among them, the PANI-HCl prepared in strong HCl acid showed the highest adsorption capacity, followed in descending order by PANI-SA, PANI-CA, PANI-TA and PANI-DI. The adsorption capacity was correlated well with oxidation state and protonation extent of PANIs. Solution pH had an obvious effect on Cr(VI) adsorption, especially for PANI-TA and PANI-DI. A mechanism of electrostatic adsorption followed by reduction of Cr(VI) to Cr(III) was proposed by analyzing FTIR, zeta potential and XPS spectra of PANIs before and after Cr(VI) adsorption.

© 2013 Elsevier B.V. All rights reserved.

## 1. Introduction

Hexavalent chromium (Cr(VI)) has drawn much attention because of its toxic and carcinogenic influences on human health and its extensive applications in industries like electroplating, mining, leather tanning and pigment production [1–4]. To meet the mandatory discharge limit of Cr(VI) (e.g. 0.5 mg/L for industrial wastewater in China) (GB 8978-1996) [5], many treatment

technologies such as reduction–precipitation, membrane separation, adsorption and solvent extraction have been developed [1–4,6–10]. Among them, adsorption has been well studied since it is efficient for simultaneous water deep purification and heavy metal recovery. Because Cr(VI) exists in water as oxyanions like  $\text{Cr}_2\text{O}_7^{2-}$ ,  $\text{HCrO}_4^-$  and  $\text{CrO}_4^{2-}$ , adsorbents that are efficient for Cr(VI) removal generally carry positively charged nitrogen-containing functional groups as the major binding site [3,4,11–13].

Polyaniline (PANI) showed many advantages of ease of synthesis, low cost, controllable conductivity and good environmental stability [14]. It has been subjected to extensive studies in battery electrodes, sensors and anticorrosion coatings. Because it carries

\* Corresponding author. Address: No. 56 Hongzhuan Road, Zhengzhou 450002, PR China. Tel./fax: +86 371 65511153.

E-mail address: [wangj12@163.com](mailto:wangj12@163.com) (J. Wang).

large amounts of amine and imine functional groups, PANI and its composites have also been used as adsorbents for inorganic and organic pollutants like Hg(II) [15], dyes [16–18] and Cr(VI) [19]. Traditionally, PANI is prepared mostly in strong protonic acids like HCl and H<sub>2</sub>SO<sub>4</sub>, with aggregated granular as the main product. Recently, PANI is also prepared in other protonic acids or neutral water to modulate its morphology, processability and conductivity [20,21]. For example, Cao et al. [22] reported for the first time that functional protonic acids such as dodecylbenzenesulfonic acid increased the solubility of PANI in common organic solvents. Zhang et al. [21] reported that morphology and electrical properties of PANI nanostructures depended on both dopant structures and reaction conditions. Trchova et al. [23] and Stejskal et al. [24] reported that depending on the acidity of the reaction solution, different PANI structures including granule, nanofiber and nanotube could be obtained. Mahanta et al. [16] reported that by changing dopants in PANI, its adsorption characteristics for anionic dyes varied. However, there exists no quantitative study evaluating the effect of protonic acids on molecular structures of PANIs, and the relationship between molecular structures of PANIs and their adsorption properties for heavy metals is yet to be clarified.

The objectives of the current study were to: (1) characterize the morphology and molecular structure of PANIs prepared by a facile sono-assisted method in various protonic acids; and (2) study the adsorption properties and associated mechanism of PANIs for aqueous Cr(VI). Five PANI samples were prepared in aqueous solutions of HCl, surfulamic acid (SA), citric acid (CA), taurine (TA) and neutral deionized (DI) water. The polymerization course of aniline was monitored by ultraviolet–visible (UV–Vis) spectra. The PANI products were characterized by scanning electron microscopy (SEM), Fourier transform infrared (FTIR) spectra, X-ray photoelectron spectroscopy (XPS), zeta potential and surface area measurements. A series of batch adsorption tests were conducted to examine the effects of pH and Cr(VI) concentration on Cr(VI) uptake. The associated mechanism was finally proposed based on adsorption tests and instrumental analyses.

## 2. Experimental

### 2.1. Materials

All chemicals in the current study were of analytical-reagent grade. Prior to use, aniline was purified by distillation under reduced pressure. Potassium dichromate (K<sub>2</sub>Cr<sub>2</sub>O<sub>7</sub>) was dried at 110 °C for 2 h. All other reagents were used as received. Ultrapure water (18.2 MΩ cm, Millipore, USA) was used throughout the adsorption tests, and diluted HCl and NaOH were used to adjust pH of Cr(VI) solutions.

### 2.2. Preparation of PANI

PANI was prepared by a facile sono-assisted chemical oxidation method. Four protonic acids (viz. HCl, SA, CA and TA) were used for comparison with pure DI water, and their structures and properties were listed in Table 1. Note that pH of the five media was in the increasing order of HCl, SA, CA, TA and DI. In a typical test, 0.911 mL (0.01 mol) of aniline was dissolved in 100 mL of 0.2 mol/L acid solutions or DI water, to which 2.282 g (0.01 mol) of ammonium peroxodisulphate was added under continuous ultrasonication (KQ-200VDE, Kunshan, China). The ultrasonication was continued for 1 h and then the mixture was allowed to stand still overnight to ensure the complete reaction. The precipitate thus formed was washed with water until water became colorless. The resultant materials were oven dried at 60 °C and kept in a

desiccator prior to use (designated as PANI-HCl, PANI-SA, PANI-CA, PANI-TA, and PANI-DI, respectively).

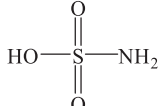
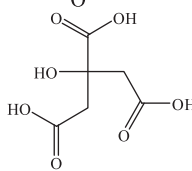
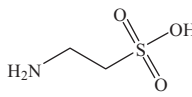
### 2.3. Sample characterization

To study the polymerization courses of aniline in different protonic acids, 0.1 mL of mixture was withdrawn at certain time intervals. After 40-fold dilution with water, the mixture was placed in a 1 cm cell of the spectrophotometer, and the UV–Vis spectra were recorded with a UV1800 spectrophotometer (Shimadzu, Japan). Surface morphologies of the as-synthesized PANIs were observed by SEM (JSM-7500F, JEOL, Japan) with 10,000- and 50,000-fold magnification. FTIR spectra were collected in 400–4000 cm<sup>-1</sup> using a Thermo Nicolet IR 200 instrument (Thermo Electron, USA). Zeta potential of the PANI suspensions (0.01 mol/L NaCl, pH range 2.5–10.5) was measured by ZetaPlus (Brookhaven Instruments, USA). Surface area and pore size of the PANIs were determined by N<sub>2</sub> adsorption–desorption at 77 K with the BET and BJH methods using an ASPA 2020 system (Micromeritics, USA). XPS measurements of PANIs before and after Cr(VI) adsorption were performed on a Thermo ESCALAB 250Xi spectrometer (Thermo Scientific, USA) with an Al Kα X-ray source (1486.6 eV photons). Both survey and high-resolution spectra of N<sub>1s</sub>, S<sub>2p</sub> and Cr<sub>2p</sub> were collected and calibrated to the binding energy (BE) of C<sub>1s</sub> at 284.6 eV. Note that unless otherwise stated, PANIs after Cr(VI) adsorption were prepared by equilibrating the as-synthesized PANIs with Cr(VI) solutions (Cr(VI) C<sub>0</sub> = 50 mg/L, pH<sub>0</sub> unadjusted, adsorbent dosage = 1 g/L, time = 24 h).

### 2.4. Batch adsorption tests

Batch tests were conducted to investigate Cr(VI) adsorption as a function of initial Cr(VI) concentration (10–300 mg/L) and aqueous pH (2–11) by the several PANI samples. Preliminary kinetic tests demonstrated that adsorption equilibrium of Cr(VI) on PANIs was achieved within approximately 24 h under the experimental conditions. Therefore, an equilibrium time of 24 h was adopted for all the adsorption experiments. To start the test, 0.04 g of PANI was mixed with 40 mL of Cr(VI) solution on a shaking table (THZ-98C, Shanghai, China) at 25 °C and 150 rpm. After reaching equilibrium, the mixture was filtered, and the filtrate was analyzed for both Cr(VI) concentration by a UV1800 spectrophotometer (Shimadzu, Japan) using 1,5-diphenylcarbazide as the complexing agent at 540 nm (GB 7467-87) [25] and total Cr concentration by

**Table 1**  
Properties of the selected acids for preparation of PANIs.

No	Acid	Structure	pK <sub>a</sub>	pH (0.2 mol/L)
1	HCl	H–Cl	–8	0.56
2	SA		1	0.72
3	CA		3.15 4.77 6.40	1.68
4	TA		1.50 9.06	5.36
5	DI	–	–	7.50

an inductively coupled plasma emission spectrometer (IRIS advantage ICP-AES, Thermo Scientific, USA). Every sample was analyzed in duplicate to guarantee accuracy of the data. Adsorption capacity ( $Q_e$ , mg/g) and Cr(VI) (or total Cr) removal rate ( $R$ , %) were obtained using the following equations:

$$Q_e = \frac{(C_0 - C_e) \times V}{M} \quad (1)$$

$$R = \frac{C_0 - C_e}{C_0} \times 100\% \quad (2)$$

where  $C_0$  and  $C_e$  (mg/L) are initial and equilibrium concentrations of Cr(VI) (or total Cr),  $V$  (L) is volume of Cr(VI) solution, and  $M$  (g) is dry mass of adsorbents.

### 3. Results and discussion

#### 3.1. Polymerization of aniline

The polymerization courses of aniline, as recorded by evolution of UV–Vis spectra and solution color with time, differed significantly among the several protonic acids (Fig. 1(a–e)). In strong acidic solutions of HCl and SA (Fig. 1(a and b)), on addition of oxidant, the reaction mixtures were first colorless and then progressively turned dark blue. Accordingly, three peaks characteristic of blue pernigraniline salt appeared at wavelengths of 300, 540, and 680 nm and become stronger with the progress of reaction [20]. After about 20 min, the bands at 540 nm and 680 nm disappeared to give rise to bands at 800 nm and 410 nm (assigned to polaron transitions) [26], while the other band at 300 nm remained constant. Meanwhile, the reaction mixtures turned dark green, indicating the formation of emeraldine salt, the final product of the aniline polymerization [27,28]. In 0.2 mol/L CA (Fig. 1(c)), a totally different variation of UV–Vis spectra and solution color was present. Throughout the 1 h polymerization, the dispersion kept bright yellow and presented two small peaks at 280 nm and 410 nm, suggesting the production of small amounts of aniline oligomers [27]. After overnight standing, however, the final UV–Vis spectra and dark-green solution color were nearly the same as that of PANI-HCl and PANI-SA. The polymerization courses in weak TA and neutral water were nearly the same (Fig. 1(d and e)). At the start of polymerization, the spectra had an extremely strong absorption at 280 nm characteristic of free aniline. This was because the pH values under both conditions (Table 1) were higher than  $pK_a$  of aniline (viz. 4.6) [24,29], making free aniline molecules the primary form of aniline monomer. After oxidant addition, the solution turned brown and turbid immediately. Accordingly, the peak at 280 nm decreased, while a new peak characteristic of aniline oligomers appeared at 410 nm. After 1 h reaction, the neutral aniline molecule was nearly exhausted, and the reaction for production of PANI was triggered as indicated from the UV–Vis spectra. The final products showed the similar UV–Vis spectra as the above PANIs, indicating that they had the similar backbone structure of emeraldine salt.

#### 3.2. Characterization of PANI

The resultant PANI samples were further characterized by SEM, FTIR, zeta potential, surface area and pore size measurements. As shown in Fig. 2, polymerization of aniline in strong HCl led to PANI aggregated particles. When we changed HCl to other weak protonic acids, nanostructured PANIs like nanoparticles and 1D nanostructures were produced. Specifically, polymerization of aniline in SA

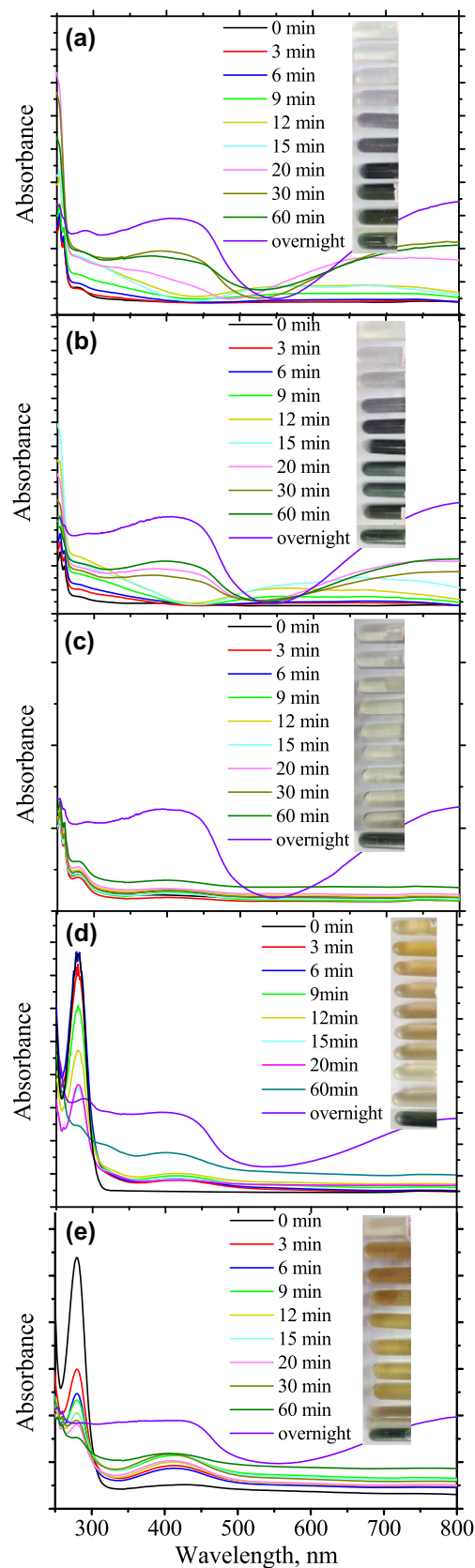


Fig. 1. Evolution of UV–Vis spectra with time during polymerization course of aniline in (a) 0.2 M HCl, (b) 0.2 M SA, (c) 0.2 M CA, (d) 0.2 M TA and (e) DI water. The insets show color change of the aqueous mixtures along with reaction time.

led to PANI nanoparticles with diameters of hundreds of nanometers, while polymerization of aniline in less acidic solutions (viz. CA and TA) and neutral water led to 1D nanostructures. Depending on the preparation media, the 1D nanostructures differed significantly in size and shape. For example, PANI-CA was straight and smooth, of ca. 150–250 nm in diameter and ca. 2.5  $\mu\text{m}$  in length. PANI-TA was relatively flexible, of ca. 80–100 nm in diameter. While PANI-DI was straight as that prepared in CA, but of a smaller diameter (ca. 100–150 nm) and a shorter length (ca. 1  $\mu\text{m}$ ). The above results demonstrated that morphology of PANIs could be controlled by simply varying the protonic acids during the sono-assisted preparation process. It was suggested that both the solution pH and the chemical structure of protonic acids could affect the PANIs' morphology. Detailed formation mechanisms of PANI nanostructures could be found in the review of Stejskal et al. [24].

Though the PANI samples differed a lot in their morphologies, they exhibited the very similar BET surface area, total pore volume and pore size distribution (Table 2). Specifically, PANI-HCl showed the lowest surface area (22.4  $\text{m}^2/\text{g}$ ) and the lowest total pore volume (0.10  $\text{cm}^3/\text{g}$ ), while PANI-TA showed the highest surface area (29.4  $\text{m}^2/\text{g}$ ) and the highest total pore volume (0.16  $\text{cm}^3/\text{g}$ ). All PANIs showed a wide pore size distribution in the range of 1.8–300 nm, and about half of the contribution to specific surface area came from the pores of 1.8–4 nm.

FTIR spectra for PANIs prepared in HCl, SA, CA, TA and DI are labeled from top to bottom (Fig. 3(A)). It was obvious the five PANIs presented similar characteristic bands at 1578, 1492, 1304, 1248, 1145 and 822  $\text{cm}^{-1}$ . These bands agreed well with the bands of PANI (emeraldine salt) reported by Trchova et al. [23] and Yan et al. [30] as shown in Table 3, suggesting the backbone of PANI prepared in this work were identical with one another and they were mostly in the form of emeraldine salt. However, there were still some obvious differences among the PANIs: (1) With decrease of solution acidity (Fig. 3(A)-a-e), the Q/B ratio (the ratio of quinoid and benzenoid units, obtained by taking area ratios of the bands at 1578 and 1492  $\text{cm}^{-1}$ ) indicating oxidation state of PANI [31] obviously decreased. (2) The characteristic absorption peaks at 1145  $\text{cm}^{-1}$  (corresponding to electron delocalization degree) and 1248  $\text{cm}^{-1}$  (corresponding to  $-\text{NH}^+$  in protonic acid doped PANI) [23,28] became lower in intensity with decreasing acidity of the preparation media. (3) In the weak acidic solution and neutral water, small peaks appeared at 1445 and 1415  $\text{cm}^{-1}$ , which were associated with phenazine-like or branched structures in aniline oligomers [23,28]. (4) Most of PANIs presented a band at 1043  $\text{cm}^{-1}$ , which could be assigned to S=O stretching in sulfonate groups (due to  $-\text{SO}_3\text{H}$  in SA and TA or sulfonation of benzene rings)

or sulfate counterions (associated with imine) [23]. The above results demonstrated that though the as-synthesized PANIs had similar backbones of emeraldine salt, they differed significantly in detailed molecular structures including oxidation state, protonation extent, electron delocalization degree and oligomer content that were expected to influence their adsorption properties.

Zeta potentials of the PANIs were measured as a function of solution pH. As shown in Fig. 4(A), the PANI-HCl, PANI-SA and PANI-CA showed the similarly shaped zeta potential versus pH curves. They had a  $\text{pH}_{\text{PZC}}$  (point of zero charge) in the range of 5.0–6.0, which was consistent with the conventional PANI in previous studies [15]. By contrast, the PANI-TA showed a lower  $\text{pH}_{\text{PZC}}$  at about 4.0, and the PANI-DI showed no  $\text{pH}_{\text{PZC}}$  in the studied pH range (i.e.  $\text{pH}_{\text{PZC}} < 2.8$ ). This indicated that the PANIs prepared in strong acidic solutions exhibited the similar surface charges with pH variation. When the preparation media were changed to weak TA or neutral DI, sulfonation of benzene rings occurred and more sites with negative charges were introduced into the PANI structures, causing the shift of  $\text{pH}_{\text{PZC}}$  to lower values.

### 3.3. Adsorption properties of Cr(VI)

#### 3.3.1. Adsorption isotherms

Fig. 5 shows Cr(VI) adsorption isotherms onto the several PANIs ( $Q_e$  versus  $C_e$  plots) at pH 4.0 (fixed by acetate buffer) at 25  $^\circ\text{C}$ . The experimentally collected equilibrium adsorption data were fitted into Langmuir and Freundlich equations:

$$\text{Langmuir: } \frac{C_e}{Q_e} = \frac{C_e}{Q_m} + \frac{1}{k_L Q_m} \quad (3)$$

$$R_L = \frac{1}{1 + k_L C_0} \quad (4)$$

$$\text{Freundlich: } \ln Q_e = \ln k_F + \frac{1}{n} \ln C_e \quad (5)$$

where  $C_e$  (mg/L) is Cr(VI) equilibrium concentration,  $Q_e$  (mg/g) is equilibrium adsorption capacity,  $Q_m$  (mg/g) is the maximum adsorption capacity,  $k_L$  and  $k_F$  are constants for the two models,  $n$  is Freundlich variable indicative of adsorption favorability, and  $R_L$  is separation factor indicative of adsorption favorability. The constants were calculated and presented in Table 4. It was observed from the correlation coefficients ( $R^2$ ) that the experimental data could be well fitted by both Langmuir and Freundlich models for all PANIs, indicating that adsorption of Cr(VI) by PANIs was not limited to just a monolayer mechanism. Depending on the protonic acids, PANIs showed different adsorption capacity and adsorption

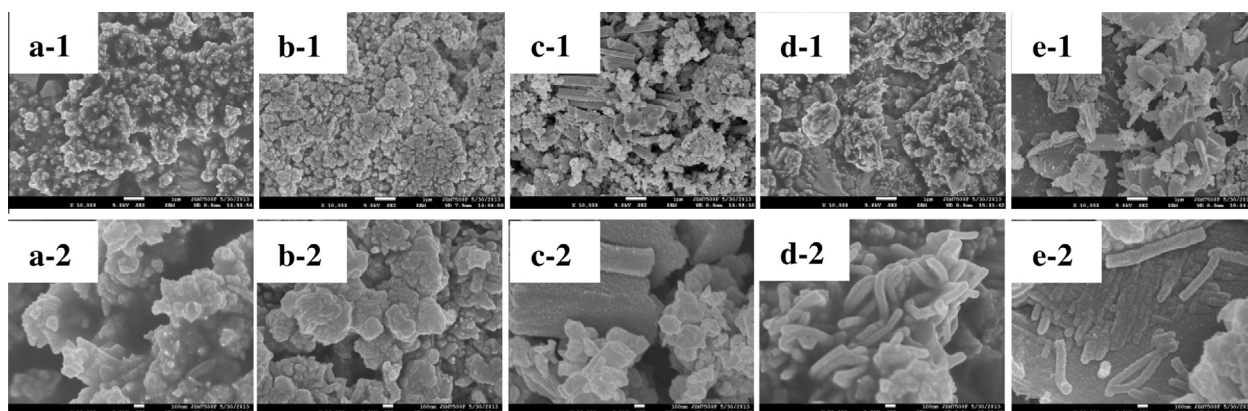
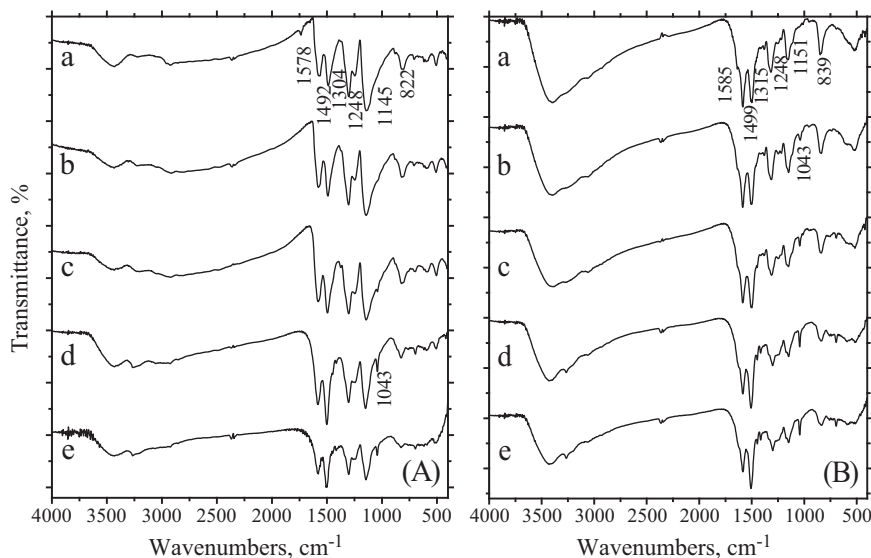


Fig. 2. SEM photographs of (a) PANI-HCl, (b) PANI-SA, (c) PANI-CA, (d) PANI-TA and (e) PANI-DI with 10,000- (upper) and 50,000-fold (lower) magnification.

**Table 2**  
Specific surface area, total pore volume and pore size distribution of the as-synthesized PANIs.

Samples	PANI-HCl	PANI-SA	PANI-CA	PANI-TA	PANI-DI
BET surface area, m <sup>2</sup> /g	22.38	23.19	24.66	29.36	24.26
Total pore volume, cm <sup>3</sup> /g	0.10	0.11	0.14	0.16	0.10
Pore size distribution, %	1.8–4 nm	45.98	47.42	41.57	48.43
	4–10 nm	19.55	18.78	15.19	17.38
	10–100 nm	27.81	28.46	35.62	33.59
	>100 nm	6.66	5.34	8.79	7.45



**Fig. 3.** FTIR spectra of (a) PANI-HCl, (b) PANI-SA, (c) PANI-CA, (d) PANI-TA and (e) PANI-DI (A) before and (B) after Cr(VI) adsorption.

**Table 3**  
Characteristic FTIR vibrational frequencies of polyaniline [23,30].

Interatomic bond	Vibrational frequency, cm <sup>-1</sup>
C=C stretching in quinoid ring	1578
C=C stretching in benzenoid ring	1492
C–N stretching in benzenoid ring	1304
C–N <sup>+</sup> stretching in protonic acid doped PANI	1248
C=N stretching in quinoid ring	1145
C–H bending out of the plane of para-substituted aromatic ring	822
S=O stretching	1043

affinity for Cr(VI). Specifically, PANI-HCl showed the highest maximum adsorption capacity ( $Q_m$  182 mg/g), followed in the descending order by PANI-SA (164 mg/g), PANI-CA (145 mg/g), PANI-TA (111 mg/g) and PANI-DI (92 mg/g). The values of  $R_L$  (in the range of 0–1) obtained from the present studies reflected the adsorption of Cr(VI) oxyanions on PANI adsorbents were favorable. The values of  $n$  (in the range of 1–10) of Freundlich model also confirmed the favorable adsorption of Cr(VI) on PANIs.

### 3.3.2. Impact of solution pH

Solution pH had a significant impact on Cr(VI) removal, with apparent inhibition observed at high pH values (Fig. 6(A)). Compared with PANI-TA and PANI-DI, the other three showed a less pronounced decrease of Cr(VI) removal ratio with the increase of  $pH_e$  (pH at adsorption equilibrium). For example, the Cr(VI) removal ratio by PANI-HCl and PANI-SA kept nearly 100% in the  $pH_e$  range of 2.0–6.0. Further increasing the solution  $pH_e$  above 7.0 slightly decreased the removal ratio to about 80%. Different

from PANI-HCl and PANI-SA, the Cr(VI) removal ratio by PANI-TA and PANI-DI decreased abruptly throughout the studied pH range, from nearly 100% at  $pH_e$  2.0 to less than 40% at  $pH_e$  8.0. Total Cr removal by PANI-HCl and PANI-TA showed a very different trend as compared with Cr(VI) removal. As shown in Fig. 6(B), the best removal of total Cr occurred at  $pH_e$  3.0–6.0 for PANI-HCl or around  $pH_e$  4.0 for PANI-TA, and further decrease or increase of  $pH_e$  significantly inhibited the total Cr removal. Throughout the studied pH range, the total Cr removal ratio was generally lower than the Cr(VI) removal ratio, especially in strong acidic solutions. For example, at  $pH_e$  2.0 the difference between the removal ratios of total Cr and Cr(VI) was the highest, i.e. about 33% for both PANIs. Similar trends of Cr(VI) removal as a function of pH were also reported for other adsorbents in previous literatures [4,13,32].

The observed impact of solution pH on Cr(VI) removal could be explained by both the electrostatic attraction mechanism between Cr(VI) oxyanions (e.g.  $CrO_4^{2-}$ ,  $HCrO_4^-$  and  $Cr_2O_7^{2-}$ ) and nitrogen-containing groups on PANIs and the reduction mechanism of Cr(VI) to Cr(III). As previously reported, both the physicochemical properties of PANI and Cr speciation substantially changed with pH variation [15]. At low pH values (e.g.  $pH < 5.0$  for PANI-HCl), nitrogen atoms of imine groups were preferentially bound by protons (as indicated by solution  $pH_e > pH_0$  (initial pH) in Fig. 6(C)), causing the PANI surfaces carrying positive charges (Fig. 4(A)) that was favorable for adsorption of anionic Cr(VI) species (primarily  $HCrO_4^-$  below pH 6.0, calculated by MINTEQA2 software, the same below). Moreover, because of high redox potential value of Cr(VI) and electron donor groups on PANI surfaces, there was a possibility that Cr(VI) anions, either in solutions or binding on the positively charged PANI surfaces, were reduced to Cr(III) (proved by further XPS analyses). And the reduction was especially facilitated with the decrease of pH since protons participated in this reaction

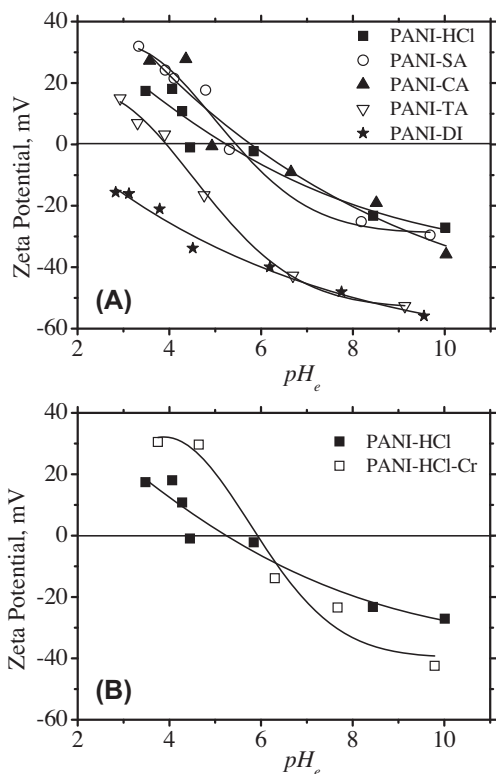


**Fig. 4.** Zeta potentials of (A) the as-synthesized PANI samples (i.e. PANI-HCl, PANI-SA, PANI-CA, PANI-TA and PANI-DI) and (B) the PANI-HCl before and after Cr(VI) adsorption (i.e. PANI-HCl-Cr) in 0.01 M NaCl.

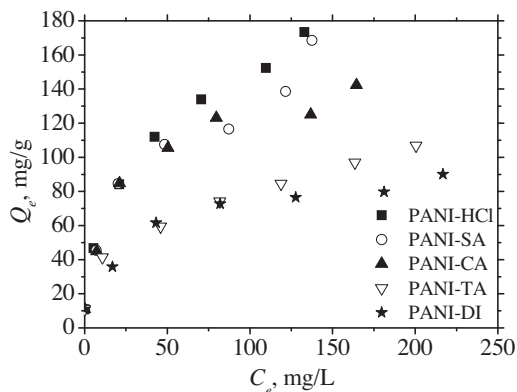


**Fig. 5.** Adsorption isotherms of PANIs for Cr(VI) at 25 °C; solution pH = 4.0 (fixed by acetate buffer), Cr(VI)  $C_0 = 10$ –300 mg/L, adsorbent dosage = 1 g/L.

**Table 4**  
Isotherm constants for Cr(VI) adsorption by PANIs at 25 °C.

Sample	Langmuir				Freundlich		
	$Q_m$	$k_L$	$R_L^a$	$R^2$	$k_F$	$n$	$R^2$
PANI-HCl	182	0.061	0.14	0.96	36.81	3.41	0.98
PANI-SA	164	0.060	0.14	0.93	36.94	3.72	0.97
PANI-CA	145	0.081	0.11	0.98	30.81	3.35	0.98
PANI-TA	111	0.043	0.19	0.95	25.61	4.03	0.97
PANI-DI	92	0.057	0.15	0.98	24.63	4.38	0.99

<sup>a</sup> The  $R_L$  values were obtained with the initial Cr(VI) concentration ( $C_0$ ) of 100 mg/L.

[33,34]. Due to the electrostatic repulsion between Cr(III) cations (primarily  $Cr^{3+}$  and  $Cr(OH)^{2+}$  below pH 4.5) and the positively charged PANIs, the resultant Cr(III) species were apt to stay in

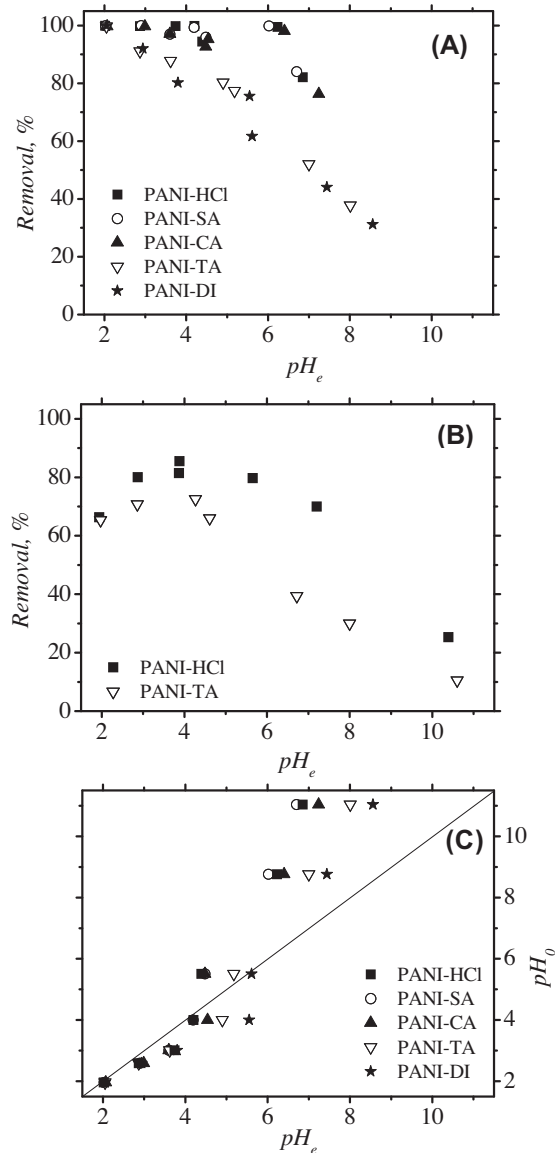


**Fig. 6.** Impact of the equilibrated solution pH ( $pH_e$ ) on (A) Cr(VI) removal and (B) total Cr removal by PANIs and (C) correlation of  $pH_e$  with the initial pH ( $pH_0$ ); solution  $pH_0 = 2$ –11 (adjusted by dilute HCl and NaOH solutions), Cr(VI)  $C_0 = 50$  mg/L, adsorbent dosage = 1 g/L.

aqueous solutions, causing the removal ratio of total Cr substantially lower than Cr(VI) at low pH values. With increasing pH, however, the imine groups underwent deprotonation (as indicated by solution  $pH_e < pH_0$  in Fig. 6(C)) and the PANIs carried negative charges (Fig. 4(A)) that was unfavorable for Cr(VI) (primarily  $CrO_4^{2-}$  above pH 6.0) adsorption. Besides, the reduction of Cr(VI) to Cr(III) (primarily  $Cr_2O_3$  precipitate above pH 5.0) was substantially inhibited at high pH values. Therefore, both Cr(VI) and total Cr removals were remarkably decreased. Competition of  $OH^-$  with Cr(VI) anions for the adsorption sites might also be responsible for the decreased Cr(VI) adsorption at high pH values. The different adsorption behaviors of the several PANIs for Cr(VI) were suggested to be due to their different molecular structures.

### 3.4. Adsorption mechanism(s) of Cr(VI) by PANI

To gain further insights into the adsorption mechanism of Cr(VI) on PANI, FTIR, zeta potential and XPS of PANI before and after

Cr(VI) adsorption were studied. As shown in Fig. 3(B), FTIR spectra of PANIs underwent several substantial changes after Cr(VI) adsorption. First, most of the FTIR bands shifted to higher wavelengths, suggesting Cr adsorbed on PANI surfaces significantly influenced the functional groups. Second, the band at  $1248\text{ cm}^{-1}$  was substantially depressed in all PANIs and the band at  $1145\text{ cm}^{-1}$  became sharper and lower in intensity. This indicated that  $-\text{NH}^+$  – in protonic acid doped PANI was the primary adsorption site for Cr(VI), and the adsorbed Cr(VI) or Cr(III) could restrict electron delocalization in PANI structure. Note that PANI-HCl, which presented the highest intensity of band at  $1248\text{ cm}^{-1}$ , showed the highest  $Q_m$  for Cr(VI). After Cr(VI) adsorption, this band disappeared in PANI-HCl and PANI-SA, while in the other PANIs this band still existed though its intensity greatly decreased. This suggested that the different adsorption properties of PANIs were correlated with the different content of  $-\text{NH}^+$  – and the different utilization efficiency of  $-\text{NH}^+$  – for Cr(VI) adsorption among the several PANIs. The full utilization of  $-\text{NH}^+$  – in PANI-HCl and PANI-SA was probably associated with the small sizes of counteranions like  $\text{Cl}^-$  and  $\text{SA}^-$ , which made anion exchange between counteranions and Cr(VI) oxyanions easier. Third, the  $Q/B$  ratio increased after Cr(VI) adsorption. For example, for PANI-HCl and PANI-SA the ratio increased above 1.0. This suggested that oxidation of the polymer backbone might accompany Cr(VI) adsorption. Fourth, the small peaks at  $1445$  and  $1415\text{ cm}^{-1}$  became stronger and even appeared in PANI-HCl and PANI-SA, indicating that adsorption of Cr(VI) could result in oxidation of PANI and consequent production of aniline oligomers. Finally, the band around  $3400\text{ cm}^{-1}$  was greatly strengthened and broadened after Cr(VI) adsorption.

Shown in Fig. 4(B) were the zeta potential versus pH curves for PANI-HCl before and after Cr(VI) adsorption. It was obvious that after Cr(VI) adsorption, the  $\text{pH}_{\text{PZC}}$  of PANI-HCl shifted to a slightly higher pH at 6.0, and the absolute values of zeta potential increased remarkably. As reported in previous studies, the specific adsorption of cationic species on solid surfaces contributed to the increased positive charge and the higher  $\text{pH}_{\text{PZC}}$ , and vice versa [35,36]. Therefore, it was reasonable to conclude that the change of surface charges of PANI-HCl was primarily due to the specific adsorption of cationic Cr(III) species which were produced from Cr(VI) reduction.

XPS spectra of PANI-HCl and PANI-TA surfaces before and after Cr(VI) adsorption were studied to gain further insights into the Cr(VI) removal mechanisms (Table 4, Fig. 7). As shown in Table 4, the as-synthesized PANI-HCl comprised 76.5% C, 9.3% N, 10.4% O, 1.7% Cl and 2.1% S, while the as-synthesized PANI-TA comprised 76.7% C, 8.8% N, 12.7% O and 1.8% S. As compared with PANI-HCl, PANI-TA showed a much lower content of dopants (sum of Cl and S) due to its lower protonation extent and lower imine content. After equilibrating PANIs with Cr(VI) solutions, the appearance of Cr was in accordance with the decrease in N, Cl and S contents, suggesting that adsorption of Cr(VI) was mainly associated with nitrogen, probably through anion exchange with the dopants in PANI structures. The different elemental contents of PANI-HCl after Cr(VI) adsorption under different pH conditions demonstrated that solution pH influenced the Cr(VI) adsorption significantly.

High-resolution spectra of  $\text{N}_{1s}$  (Fig. 7(A)) showed that before Cr(VI) adsorption,  $\text{N}_{1s}$  of PANI-HCl (Fig. 7(A)-a) could be fitted into two peaks at 399.6 and  $>400.0\text{ eV}$ , corresponding to nitrogen atoms in amine ( $-\text{NH}-$ ) (N2) and doped imine ( $-\text{NH}^+-$ ) (N1) functional groups, respectively [15,37]. Close peak areas for these two nitrogen species demonstrated that PANI-HCl was in its emeraldine salt state [14,37]. After Cr(VI) adsorption at three different pH values (i.e.  $\text{pH}_e$  2.0, 4.7 and 9.5), the total N content decreased from 9.3 atom% to 8.8, 8.6 and 9.1 atom%, respectively. Besides, of the two

peaks N2 stayed relatively constant, while N1 substantially decreased and even disappeared after Cr(VI) adsorption at  $\text{pH}_e$  9.5. Simultaneously, a new peak appeared at 398.3 eV which could be assigned to imine group ( $-\text{N}=\text{}$ ) (N3, at  $\text{pH}_e$  4.7 and 9.5) [15]. In contrast to PANI-HCl, PANI-TA presented a much lower N1 content than N2, and after Cr(VI) adsorption at  $\text{pH}_e$  4.6, N1 was completely transformed to N3. Analyses of  $\text{N}_{1s}$  spectra indicated that protonic acids significantly affected the PANI molecular structures (e.g. imine content or  $Q/B$  ratio and protonation extent) and the Cr(VI) removal process associated closely with the nitrogen groups (especially the imine group). In agreement with deprotonation of imine nitrogen,  $\text{Cl}_{2p}$  and  $\text{S}_{2p}$  peaks were significantly decreased after Cr(VI) adsorption, and the decrease correlated well with the solution pH. Peak fitting of  $\text{Cl}_{2p}$  (Fig. 7(B)) demonstrated that Cl in PANI-HCl existed primarily in three forms: chloride anion (Cl1), anionic chloride resulting from the charge transfer between chlorine and PANI chain (Cl2) and covalently bonded chlorine (Cl3) [15]. After Cr(VI) adsorption at  $\text{pH}_e$  2.0, Cl1 was greatly decreased, causing substantial decrease in total Cl content from 1.7 to 1.3 atom% (Table 5). Because the proton concentration was extremely high at such a low pH, we suggested the decrease of Cl1 was primarily because of the anion exchange between  $\text{Cl}^-$  and Cr(VI) anions. When Cr(VI) adsorption occurred at  $\text{pH}_e$  4.7 and 9.5, Cl1 completely disappeared due to both the anion exchange and the deprotonation reactions and the residual chlorine (0.4 atom%) was mainly in covalent-bond chlorine form. In contrast with  $\text{Cl}_{2p}$ ,  $\text{S}_{2p}$  spectra ( $\text{S}_{2p3/2}$  168.3 eV, assigned to  $-\text{SO}_3\text{H}$  and  $\text{SO}_4^{2-}$ , Fig. 7(C)) [38] were relatively stable, probably due to the larger size of

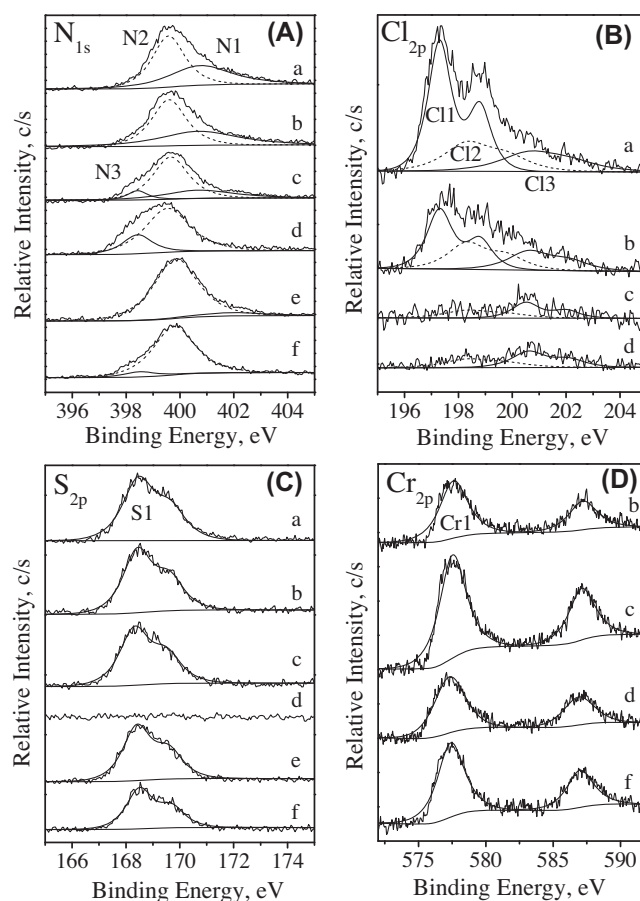
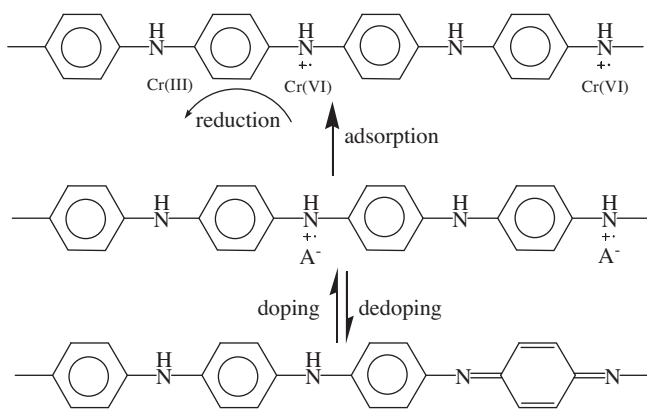


Fig. 7. XPS spectra of high-resolution scan of (A)  $\text{N}_{1s}$ , (B)  $\text{Cl}_{2p}$ , (C)  $\text{S}_{2p}$  and (D)  $\text{Cr}_{2p}$  for PANI-HCl (a) before and after Cr(VI) adsorption at (b)  $\text{pH}_e$  2.0 and (c)  $\text{pH}_e$  4.7, (d)  $\text{pH}_e$  9.5 and PANI-TA (e) before and after Cr(VI) adsorption at (f)  $\text{pH}_e$  = 4.6.

**Table 5**  
Distribution of C, N, O, Cl, S and Cr on PANI surfaces (a) before and (b) after Cr(VI) adsorption.

		Atomic concentration, %					
		C	N	O	Cl	S	Cr
PANI-HCl	Before Cr(VI) adsorption	76.5	9.3	10.4	1.7	2.1	-
	@ pH <sub>e</sub> 2.0	72.5	8.8	14.1	1.3	2.0	1.3
	After adsorption	69.2	8.6	17.6	0.4	2.0	2.2
	@ pH <sub>e</sub> 9.5	77.2	9.1	11.8	0.4	0.2	1.3
PANI-TA	Before Cr(VI) adsorption	76.7	8.8	12.7	-	1.8	-
	After adsorption	73.7	8.4	15.1	-	1.3	1.5
	@ pH <sub>e</sub> 4.6						



**Scheme 1.** The proposed adsorption mechanisms of Cr(VI) on PANIs.

sulfate anions and stronger bonding of sulfonate groups. High-resolution spectra of Cr<sub>2p</sub> (Fig. 7(D)) could be fitted with only one doublet-peak with Cr<sub>2p<sub>3/2</sub></sub> being situated at 577.6 eV, which could be assigned to Cr(III) (Cr1) [4,39]. This indicated that the adsorbed Cr on PANI-HCl and PANI-TA existed primarily in its trivalent form, implying that the adsorption process involved the full reduction of Cr(VI) to Cr(III). Similar observations for Cr(VI) reduction were also reported for adsorbents including fibrous adsorbent [4], biomass [39–41] and polyaniline [33]. By comparison of the Cr content (Table 5), it could be concluded that PANI-HCl showed better adsorption properties than PANI-TA and the optimal adsorption of total Cr occurred in weak acidic solutions.

Based on this study, we proposed an adsorption followed by reduction mechanism of Cr(VI) uptake by PANIs shown in Scheme 1. When mixing Cr(VI) solutions with PANIs, the electrostatic interaction between protonated imine groups on the adsorbent surface with aqueous Cr(VI) oxyanions caused Cr(VI) adsorption on PANI surface. Any factors (e.g. PANI preparation conditions, water chemistry conditions) that influenced the physicochemical properties of PANI and Cr speciation would influence the Cr(VI) adsorption. Depending on the protonic acids, the as-prepared PANIs differed in their detailed molecular structures including oxidation state, protonation extent and oligomer content etc. and surface charges. Because protonated imine groups were the primary adsorption sites for Cr(VI) and electrostatic interaction was the primary adsorption mechanism, PANIs prepared in strong HCl, SA, and CA solutions presenting the highest *Q/B* ratio, the highest protonation extent and the highest pH<sub>PZC</sub> showed the best adsorption capacity for Cr(VI). The impact of solution pH on Cr(VI) was due to the deprotonation of imine groups under high pH values and the competitive adsorption of OH<sup>-</sup> with Cr(VI) oxyanions. Because of the strong oxidizing ability of Cr(VI), we proposed that Cr(VI) adsorbed on PANI surfaces could react with the PANIs and consequently caused the full reduction of Cr(VI) to Cr(III) and the production of peroxidation products like fully oxidized pernigraniline and aniline oligomers.

## 4. Conclusion

We have successfully prepared various nanostructured PANIs with different morphologies, molecular structures, surface charges and adsorption properties by changing the acidity and protonic acids of the preparation media through a facile sono-assisted method. The PANI nanoparticles prepared in strong HCl and SA acids presented the highest ratio of quinoid and benzenoid units, the highest extent of protonation and a relatively high pH<sub>PZC</sub>. While the PANI 1D nanostructures prepared in weak acids and neutral water contained higher contents of aniline oligomers and carried more negative charges. The different surface charges and molecule structures, especially the different content and efficiency of protonated imine groups, were deemed as the primary reasons for varied adsorption properties of PANIs for aqueous Cr(VI). Based on FTIR and XPS spectra, a mechanism of electrostatic adsorption followed by reduction of Cr(VI) to Cr(III) was proposed for Cr(VI) uptake by PANIs. Findings of the current study have profound application in tuning PANI structures by protonic acids for removal of heavy metals from polluted waters.

## Acknowledgments

Funding for this research was provided by the National Natural Science Foundation of China (grant 21107021) and the Plan for Scientific Innovation Talent of Henan Province (grants 134100510020, 124200510023). The anonymous reviewers are gratefully acknowledged for their valuable comments and suggestions that help to substantially improve this manuscript.

## References

- [1] K.C.K. Lai, I.M.C. Lo, Removal of chromium(VI) by acid-washed zero-valent iron under various groundwater geochemistry conditions, *Environ. Sci. Technol.* 42 (2008) 1238–1244.
- [2] N. Shevchenko, V. Zaitsev, A. Walcarius, Bifunctionalized mesoporous silicas for Cr(VI) reduction and concomitant Cr(III) immobilization, *Environ. Sci. Technol.* 42 (2008) 6922–6928.
- [3] J. Wang, X. Lv, L. Zhao, J. Li, Removal of chromium from electroplating wastewater by aminated polyacrylonitrile fibers, *Environ. Eng. Sci.* 28 (2011) 585–589.
- [4] J. Wang, L. Zhao, W. Duan, L. Han, Y. Chen, Adsorption of aqueous Cr(VI) by novel fibrous adsorbent with amino and quaternary ammonium groups, *Ind. Eng. Chem. Res.* 51 (2012) 13655–13662.
- [5] GB 8978–1996. State Environmental Protection Agency of China: Beijing, 1996 (in Chinese).
- [6] G. Almaguer-Busso, G. Velasco-Martínez, G. Carreño-Aguilera, S. Gutiérrez-Granados, E. Torres-Reyes, A. Alatorre-Ordaz, A comparative study of global hexavalent chromium removal by chemical and electrochemical processes, *Electrochem. Commun.* 11 (2009) 1097–1100.
- [7] S. Sachdeva, A. Kumar, Synthesis and modeling of composite poly(styrene-co-acrylonitrile) membrane for the separation of chromic acid, *J. Membr. Sci.* 307 (2008) 37–52.
- [8] S. Deng, Y. Ting, Polyethylenimine-modified fungal biomass as a high-capacity biosorbent for Cr(VI) anions: Sorption capacity and uptake mechanisms, *Environ. Sci. Technol.* 39 (2005) 8490–8496.
- [9] A.K. Bhattacharya, T.K. Naiya, S.N. Mandal, S.K. Das, Adsorption, kinetics and equilibrium studies on removal of Cr(VI) from aqueous solutions using different low-cost adsorbents, *Chem. Eng. J.* 137 (2008) 529–541.



- [10] F.J. Alguacil, M. Alonso, F.A. Lopez, A. Lopez-Delgado, I. Padilla, Dispersion-free solvent extraction of Cr(VI) from acidic solutions using hollow fiber contactor, *Environ. Sci. Technol.* 43 (2009) 7718–7722.
- [11] P.A. Kumar, S. Chakraborty, M. Ray, Removal and recovery of chromium from wastewater using short chain polyaniline synthesized on jute fiber, *Chem. Eng. J.* 141 (2008) 130–140.
- [12] J. Wang, K. Pan, Q. He, B. Cao, Polyacrylonitrile/polypyrrole core/shell nanofiber mat for the removal of hexavalent chromium from aqueous solution, *J. Hazard. Mater.* 244–245 (2013) 121–129.
- [13] Y. Zheng, W. Wang, D. Huang, A. Wang, Kapok fiber oriented-polyaniline nanofibers for efficient Cr(VI) removal, *Chem. Eng. J.* 191 (2012) 154–161.
- [14] J.Y. Shimano, A.G. MacDiarmid, Polyaniline, a dynamic block copolymer: Key to attaining its intrinsic conductivity?, *Synth. Met.* 123 (2001) 251–262.
- [15] J. Wang, B. Deng, H. Chen, X. Wang, J. Zheng, Removal of aqueous Hg(II) by polyaniline: Sorption characteristics and mechanisms, *Environ. Sci. Technol.* 43 (2009) 5223–5228.
- [16] D. Mahanta, G. Madras, S. Radhakrishnan, S. Patil, Adsorption and desorption kinetics of anionic dyes on doped polyaniline, *J. Phys. Chem. B* 113 (2009) 2293–2299.
- [17] M. Ayad, G. El-Hefnawy, S. Zaghlol, Facile synthesis of polyaniline nanoparticles; its adsorption behavior, *Chem. Eng. J.* 217 (2013) 460–465.
- [18] J. Wang, X. Han, H. Ma, Y. Ji, L. Bi, Adsorptive removal of humic acid from aqueous solution on polyaniline/attapulgite composite, *Chem. Eng. J.* 173 (2011) 171–177.
- [19] X. Guo, G. Fei, H. Su, L. Zhang, High-performance and reproducible polyaniline nanowire/tubes for removal of Cr(VI) in aqueous solution, *J. Phys. Chem. C* 115 (2011) 1608–1613.
- [20] M. Chakraborty, D.C. Mukherjee, B.M. Mandal, Dispersion polymerization of aniline in different media: A UV-Visible spectroscopic and kinetic study, *Langmuir* 16 (2000) 2482–2488.
- [21] Z. Zhang, Z. Wei, M. Wan, Nanostructures of polyaniline doped with inorganic acids, *Macromolecules* 35 (2002) 5937–5942.
- [22] Y. Cao, P. Smith, A.J. Heeger, Counter-ion induced processibility of conducting polyaniline and of conducting polyblends of polyaniline in bulk polymers, *Synth. Met.* 48 (1992) 91–97.
- [23] M. Trchova, I. Sedenkova, E.N. Konyushenko, J. Stejskal, P. Holler, G. Ciric-Marjanovic, Evolution of polyaniline nanotubes: The oxidation of aniline in water, *J. Phys. Chem. B* 110 (2006) 9461–9468.
- [24] J. Stejskal, I. Sapurina, M. Trchová, Polyaniline nanostructures and the role of aniline oligomers in their formation, *Prog. Polym. Sci.* 35 (2010) 1420–1481.
- [25] GB 7467–87. State Environmental Protection Agency of China: Beijing, 1987 (in Chinese).
- [26] J. Stejskal, P. Kratochvil, N. Radhakrishnan, Polyaniline dispersions 2. UV-Vis absorption spectra, *Synth. Met.* 61 (1993) 225–231.
- [27] Y. Wang, H.D. Tran, L. Liao, X. Duan, R.B. Kaner, Nanoscale morphology, dimensional control, and electrical properties of oligoanilines, *J. Am. Chem. Soc.* 132 (2010) 10365–10373.
- [28] Z.D. Zujovic, Y. Wang, G.A. Bowmaker, R.B. Kaner, Structure of ultralong polyaniline nanofibers using initiators, *Macromolecules* 44 (2011) 2735–2742.
- [29] M. Ilic, E. Koglin, A. Pohlmeier, H.D. Narres, M.J. Schwuger, Adsorption and polymerization of aniline on Cu(II)-montmorillonite: Vibrational spectroscopy and ab Initio calculation, *Langmuir* 16 (2000) 8946–8951.
- [30] X. Yan, Z. Han, Y. Yang, B. Tay, Fabrication of carbon nanotube-polyaniline composites via electrostatic adsorption in aqueous colloids, *J. Phys. Chem. C* 111 (2007) 4125–4131.
- [31] D.W. Hatchett, M. Josowicz, J. Janata, Acid doping of polyaniline: Spectroscopic and electrochemical studies, *J. Phys. Chem. B* 103 (1999) 10992–10998.
- [32] R. Zhang, H. Ma, B. Wang, Removal of chromium(VI) from aqueous solutions using polyaniline doped with sulfuric acid, *Ind. Eng. Chem. Res.* 49 (2010) 9998–10004.
- [33] A. Olad, R. Nabavi, Application of polyaniline for the reduction of toxic Cr(VI) in water, *J. Hazard. Mater.* 147 (2007) 845–851.
- [34] S.T. Farrell, C.B. Breslin, Reduction of Cr(VI) at a polyaniline film: Influence of film thickness and oxidation state, *Environ. Sci. Technol.* 38 (2004) 4671–4676.
- [35] A. Chakir, J. Bessiere, K.E.L. Kacemi, B. Marouf, A comparative study of the removal of trivalent chromium from aqueous solutions by bentonite and expanded perlite, *J. Hazard. Mater.* B95 (2002) 29–46.
- [36] G. Zelmanov, R. Semiat, Iron (Fe<sup>+3</sup>) oxide/hydroxide nanoparticles-based agglomerates suspension as adsorbent for chromium (Cr<sup>+6</sup>) removal from water and recovery, *Sep. Purif. Technol.* 80 (2011) 330–337.
- [37] E.T. Kang, K.G. Neoh, K.L. Tan, Polyaniline: a polymer with many interesting intrinsic redox states, *Prog. Polym. Sci.* 23 (1998) 277–324.
- [38] X.L. Wei, M. Fahlman, A.J. Epstein, XPS Study of highly sulfonated polyaniline, *Macromolecules* 32 (1999) 3114–3117.
- [39] D. Park, Y.S. Yun, J.M. Park, XAS and XPS studies on chromium-binding groups of biomaterial during Cr(VI) biosorption, *J. Colloid Interface Sci.* 317 (2008) 54–61.
- [40] V.M. Boddur, K. Abburi, J.L. Talbott, E.D. Smith, Removal of hexavalent chromium from wastewater using a new composite chitosan biosorbent, *Environ. Sci. Technol.* 37 (2003) 4449–4456.
- [41] M. Panda, A. Bhowal, S. Datta, Removal of hexavalent chromium by biosorption process in rotating packed bed, *Environ. Sci. Technol.* 45 (2011) 8460–8466.